The equilibrium oceanic microseism spectrum

Spahr C. Webb
Scripps Institution of Oceanography, University of California, San Diego, La Jolla, California 92093

(Received 4 February 1992; accepted for publication 18 May 1992)

Microseisms are seismoacoustic waves excited by nonlinear interactions of ocean waves and are evident in the band 0.1 to 5 Hz in measurements of pressure or displacement spectra from the deep seafloor. A remarkable uniformity in microseism amplitudes is observed at the seafloor, despite many orders of magnitude variation in the amplitude of ocean waves overhead. This paper looks at how a balance is established between the excitation of microseisms under large source regions and the dissipation of this energy within a waveguide formed by the ocean, crust, and upper mantle. The excitation functions and dissipation of modes within ocean models are calculated to determine the "equilibrium microseism spectrum" of displacement or pressure for which local excitation is balanced by local dissipation. Efficient propagation of energy within the ocean waveguide also acts to make deep ocean microseism observations homogeneous.

PACS numbers: 43.30.Ma, 43.30.Nb

INTRODUCTION

The term "microseism" originally referred to the ever-present 6- to 8-s noise observed on seismographs worldwide. This signal is caused by waves at sea, as has been demonstrated by a plethora of investigations. This paper is concerned with the microseism signal detected by seismometers and pressure gauges within the sea and on and under the sea bed. Longuet-Higgins (1950) first showed how the interaction of pairs of surface gravity waves propagating in opposite directions could lead to the excitation of high phase velocity (acoustic) components. In the nonlinear microseism excitation mechanism, two ocean waves of similar frequency interact to drive an elastic wave at twice the frequency. The microseism spectrum is therefore intimately related to the ocean surface wave spectrum. The source function for microseisms is well understood; a recent review is provided by Kibblewhite and Wu (1991).

For the most part researchers have been satisfied in comparing the source function to measurements as though the measurements were made in an ocean of infinite depth or above a perfectly absorbing seabed. The rapid rise in elastic wave velocities with depth below the seafloor establishes an efficient waveguide within the ocean and crust at microseism frequencies (0.05 to 5 Hz) so that microseisms from storms far out at sea are detected on land in the center of the continents. This paper examines the role of this waveguide in establishing the microseism spectrum seen at the sea bed.

A description of the microseism spectrum at any point on the seafloor depends on a description of the ocean wave spectrum over a large area, since elastic waves propagate hundreds of kilometers within the ocean-seafloor waveguide. The size of this area for any frequency can be predicted from models of propagation of modes within the waveguide. Rather than predicting the microseism spectrum at a site from a detailed description of the ocean wave field at a single time, one can look to climatological descriptions of the ocean wave spectrum over the ocean to predict the "climatology of microseisms" at a site.

Measurements of pressure or displacement spectra from the seafloor from different locations, seasons and under different sea states look remarkably similar in shape and amplitude (Fig. 1). There appears to be an "equilibrium microseism" spectrum, and the microseism spectrum seems to quickly evolve to this equilibrium shape. This paper shows how this equilibrium shape is established under large source regions and examines how large a source region must be for the spectrum to approach the equilibrium spectrum. In extensive source regions, each mode grows in amplitude until

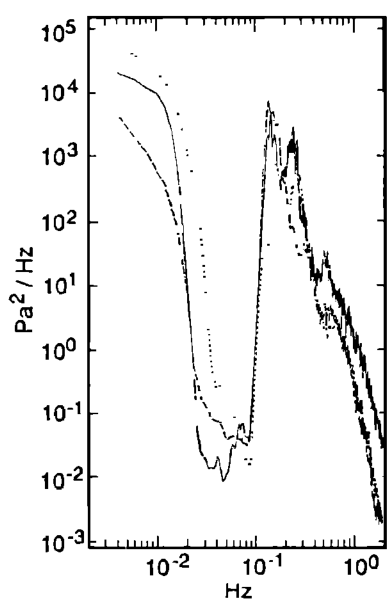

FIG. 1. The spectrum of pressure fluctuations from three sites from the seafloor in the eastern Pacific in the band from 0.002 to 2 Hz. The microseism peak is apparent in each spectrum above 0.1 Hz.

Downloaded 30 Jul 2011 to 134.246.166.168. Redistribution subject to ASA license or copyright; see http://asadl.org/journals/doc/ASALIB-home/info/terms.

the rate of excitation is balanced by dissipation. The excitation rate can be nearly uniform over large areas of the ocean surface because the ocean wave spectrum evolves to a shape which above some limiting frequency is nearly independent of wind velocity (for large fetch). The ocean wave spectrum is sometimes termed "saturated" under these conditions, and one might also use the term for the equilibrium microseism spectrum. The existence of an equilibrium spectrum simplifies the comparison between ocean wave climatology and microseism climatology. The universality of the amplitude and shape of the equilibrium spectrum is maintained over most of the possible range of earth models because the differences in excitation and dissipation in models of the deep seafloor are small, on the order of 10 dB.

Analyses of a 3-yr-long record of seafloor noise obtained from a fixed array of hydrophones (McCreery and Duennebier, 1988; McCreery *et al.*, 1991) show clearly the saturation of the microseism spectrum at frequencies above 1 Hz. Energy in the band from 1 to 5 Hz was found to be independent of wind speed at wind speeds above 10 m/s. The energy was fixed at a level 10 to 15 dB higher than the energy detected during intervals of calm winds.

There have been several efforts directed at estimating the excitation of microseisms in a realistic oceanic waveguide. Hasselmann (1963) showed how to predict the amplitude of microseisms detected on land associated with seismic surface waves excited by storms at sea for a simple earth model. Recently, Adair (1985) used waveform modeling techniques to predict the ocean floor microseism spectrum but used an unphysical source at the seafloor in his calculations with a proscribed correlation function at the seafloor. The result depended on the choice of the correlation function and the crucial role played by attenuation was ignored. Schmidt and Kuperman (1988) also use full waveform modeling techniques to calculate the trapping of energy in the ocean waveguide. They found the amplification of the pressure spectrum in shallow water associated with trapping of energy in the waveguide could be as great as 30 dB over the pressure spectrum calculated for an ocean of infinite depth. Their calculations necessarily ignore teleseismic (remote) microseisms, and although the earth model used in the paper was inappropriate for most deep water sites, their results agree generally with the results presented here. This paper takes a different approach, focusing on the physical mechanisms associated with the excitation of energy within the waveguide, and the role of finite source regions.

I. MICROSEISM GENERATION IN AN OCEAN OF INFINITE DEPTH

The section reviews work on the excitation of microseisms by interaction of opposing wave trains of surface gravity waves. The mechanism has been investigated by a multitude of researchers, Kibblewhite and Wu (1991) provide a recent review of work on this problem. These authors also discuss and dismiss recent papers disputing wave–wave interaction as the primary source of microseisms in the band from 0.1 to 5 Hz. At lower frequencies a different mechanism generates a second microseism peak of lesser amplitude centered at about 0.07 Hz. Above 5 Hz, noise may be generated by breaking waves (Duennebier *et al.*, 1986) and by shipping. Only microseisms generated by the wave interaction mechanism are considered in this paper.

A perturbation analysis is the standard procedure for calculating the wave–wave interaction mechanism resulting in microseisms. The equations describing the propagation of ocean surface waves are nonlinear at second order. The quadratic nonlinearity allows a triad interaction between a pair of surface gravity waves and a high phase velocity elastic wave if the two surface gravity waves are of similar frequency and traveling in nearly opposing directions so that the difference in wave numbers is small. The frequency of the elastic wave excited by this mechanism is equal to the sum of the frequencies of the two surface gravity waves and hence equal to nearly twice the frequency of the surface waves. These elastic waves can be described as acoustic waves in the ocean, but significant energy propagates below the seabed and waves are more appropriately termed seismoacoustic waves. The modes associated with the elastic waves can be variously termed Rayleigh waves, ocean acoustic modes, or Stoneley waves. Wave–wave interaction can also force waves which propagate more slowly than acoustic waves in the ocean. These waves decay evanescently with depth from the surface, but can be an important component of the microseism signal near the ocean surface.

The ocean wave field can be described by a power spectrum of surface elevation in frequency and direction $H(\omega,\theta)$. The wave number is given by the surface gravity wave dispersion relation. Hasselmann (1963) showed how the ocean wave spectrum could be used to predict the excitation of microseisms. The microseism excitation is described as a distributed pressure field just below the free surface with a wave number and frequency spectrum $\xi(\omega,k)$ that under some approximations can be related to the ocean wave spectrum:

$$\xi(\omega,k) = \frac{\rho^2 g^2 \omega}{2} \int_0^{2\pi} H\left(\frac{\omega}{2},\theta\right) H\left(\frac{\omega}{2},\theta+\pi\right) d\theta, \quad (1)$$

where ρ is the density of seawater. This spectrum is independent of wave number, an approximation valid for wave numbers small compared to wave numbers of surface gravity waves. Jacobs *et al.* (1990) have recently investigated the full wave-number dependence of ξ in variously simulated surface wave fields. They find the approximation of an uniform spectrum of pressure in wave number near the sea surface is a poor model for surface wave fields dominated by highly directional components such as swell from distant storms, but otherwise not unreasonable. A spectrum that is white in wave number corresponds to a correlation function that is a delta function in space coordinates:

$$\langle p(\mathbf{x},\omega) p^*(\mathbf{x}',\omega) \rangle = \int\int \xi(\omega,\mathbf{k}) e^{i\mathbf{k}\cdot\mathbf{x}} \, d\mathbf{k}$$
$$= C(\omega)\delta(|\mathbf{x}-\mathbf{x}'|); \quad (2)$$

$$C(\omega) = \frac{4\pi^2 \rho^2 g^2 \omega}{2} \int_0^{2\pi} H\left(\frac{\omega}{2},\theta\right) + H\left(\frac{\omega}{2},\theta+\pi\right) d\theta. \quad (3)$$

Downloaded 30 Jul 2011 to 134.246.166.168. Redistribution subject to ASA license or copyright; see http://asadl.org/journals/doc/ASALIB-home/info/terms.

The correlation function is a more convenient description with the Green's function techniques used later in this paper. The delta function is an approximation valid for scales large compared to the wavelengths of ocean surface waves.

The acoustic wave equation is used to propagate the signal to depth. At the low frequencies considered here, the speed of sound can be taken as a constant within the ocean so that the two solutions for propagation within the ocean become

$$p = e^{i(\mathbf{k}\cdot\mathbf{x} - \omega t)}[ae^{irz} + be^{-irz}]; \quad r = [(\omega/\alpha)^2 - k^2]^{1/2}. \tag{4}$$

The evanescent and propagating components correspond to real and imaginary values of r. For horizontal wave numbers that are large compared to acoustic wave numbers, the vertical wave number is imaginary and the solution must decay away from the source at the sea surface. At great depth in the ocean these components are absent. The usual next step is to look at the limit of infinite depth and integrate over only those wave numbers in the source spectrum for which $k < \omega/\alpha$, (over all waves which propagate as acoustic waves in the ocean; Tyler *et al.*, 1974). The pressure frequency spectrum deep within the ocean is then

$$P(\omega) = \int_0^{2\pi} \int_0^{\omega/\alpha} \xi(\omega,k) k\, dk\, d\theta, \tag{5}$$

$$P(\omega) = \frac{\pi \rho^2 g^2 \omega^3}{2\alpha^2} \int_0^{2\pi} H\left(\frac{\omega}{2},\theta\right) H\left(\frac{\omega}{2},\theta + \pi\right) d\theta. \tag{6}$$

Kibblewhite and Wu (1991) describe modifications to the acoustic wave equation and to the ω/α limit, when the effect of gravity is included. The effect of the evanescent fraction is apparent in acoustic measurements made near the free surface by a slowly profiling instrument (Cox and Jacobs, 1989). Near the sea surface, waves with wave numbers as large as order $1/h$ can generate significant pressure signal at depth h. Integrating the source spectrum over all wave numbers $k < 1/h$ leads to an inverse square law with depth for the variance in the microseism peak in agreement with the observations.

The frequency spectrum of vertical displacement within an ocean of infinite depth can also be calculated:

$$W(\omega) = \int_0^{2\pi} \int_0^{\omega/\alpha} \frac{\xi(\omega,k)[(\omega/\alpha)^2 - k^2]}{\rho^2 \omega^4} k\, dk\, d\theta,$$

$$W(\omega) = \frac{\pi g^2 \omega}{4\alpha^4} \int_0^{2\pi} H\left(\frac{\omega}{2},\theta\right) H\left(\frac{\omega}{2},\theta + \pi\right) d\theta. \tag{7}$$

The results from Eqs. (6) and (7) will be compared to results from the mode calculations to estimate the "gain" within the waveguide, following Schmidt and Kuperman (1988).

Equations (6) and (7) leave out the problem of the interaction of the acoustic waves with the seabed. The spectra predicted from these calculations are correct if no energy is reflected at the seabed. Energy is reflected either at the seabed or below the seafloor in a vertically stratified model. At some wave numbers, the phase of the reflected wave will create a node at the free surface corresponding to the normal modes of the ocean-seafloor waveguide. The modes are excited much as a resonant oscillator so that after initiation, each mode grows linearly with time until limited by dissipation or the extent of the source region (Hasselmann, 1963).

If the pressure field over the entire free surface were known, the Fourier transform in frequency of the pressure at the seabed could be calculated from the Fourier transform of the surface pressure field $\zeta(k,\omega)$ from an equation of the form:

$$p(\mathbf{x},\omega) = \int \frac{\zeta(\mathbf{k},\omega) e^{i(\mathbf{k}\cdot\mathbf{x} - \omega t)}}{B(\mathbf{k},\omega)} d\mathbf{k}, \tag{8}$$

because the problem is linear (Lighthill, 1978). At a given frequency, discrete values of wave number are associated with the resonantly forced modes corresponding to the poles of B. The residues at these poles should depend on the attenuation coefficients of the individual modes. Also in this equation is a finite response under the source region due to the nonresonant components of the forcing. In limited regions, (shallow water, closed basins) and during the initial stages after the onset of the wind, the nonresonant components determine the microseism spectrum seen at the seafloor because the resonant components grow with time and fetch. The nonresonate components must decay with distance outside of the source region. The result for the pressure spectrum in an ocean of infinite depth [Eq. (6)] provides an estimate for the nonresonant (local) pressure component. This is equivalent to setting $B = 1$ for $k < \omega/\alpha$, corresponding to no reflection at the seafloor and infinite dissipation within the seafloor. Equation (8) can be used as an estimate of the nonresonant component of the displacement, if the seafloor is taken as a fluid layer with the same acoustic velocity as seawater.

A model of the ocean surface wave spectrum is required to complete the calculations. In most models, the ocean surface wave spectrum maintains a constant shape under increasing wind (Fig. 2). The amplitude of the spectrum at the higher frequencies remains nearly invariant, the wave spectrum evolves with wind velocity as energy is transferred to lower frequency, larger amplitude components. Equation (6) shows the microseism spectrum is directly related to the

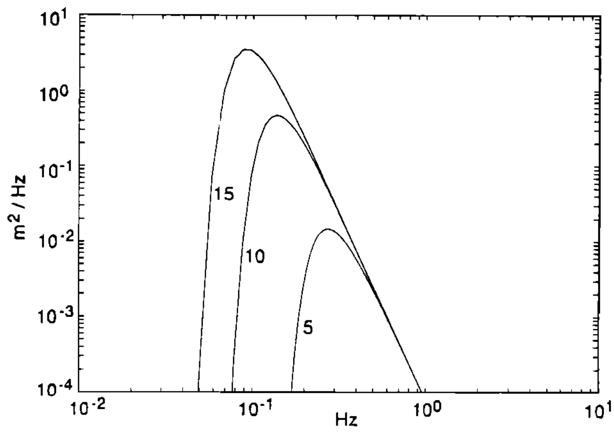

FIG. 2. The wave height spectrum in the Peirson–Moskowitz model for a fully developed sea under wind velocities of 5, 10, and 15 m/s.

Downloaded 30 Jul 2011 to 134.246.166.168. Redistribution subject to ASA license or copyright; see http://asadl.org/journals/doc/ASALIB-home/info/terms

ocean wave spectrum but with a doubling of frequency associated with the quadratic nonlinearity. A saturated shape to the ocean wave spectrum seems to predict an saturated shape to the microseism spectrum. However, it will be shown later that the existence of an apparently saturated spectrum for microseisms also depends on the properties of the oceanic waveguide.

There are several commonly used models for the ocean wave height spectrum. The Pierson and Moskowitz spectrum (1964) will be used in this paper since it is a prediction for a "fully developed sea." More recent formulations such as the JONSWAP spectrum (Hasselmann *et al.*, 1973) provide a better description of the spectrum in regions of limited fetch, or for wind events of short duration. The JONSWAP spectrum more accurately predicts a peaking in the microseism spectrum (an "overshoot") associated with the lowest frequency waves in the wind driven component of a developing ocean wave field. The ocean wave spectrum changes shape from the very peaked JONSWAP spectrum at the start of a wind event, to the broader Peirson and Moskowitz shape under a persistent wind (Donelan *et al.*, 1985). The ocean wave field evolves toward a fully developed sea state in less than a day under gale force winds. The difference in the height of the spectral peak from a "young" to an "old" sea can be 10 dB, suggesting a nearly 20-dB variation in microseism amplitudes. These changes in spectral shape seem to be mirrored in measurements of microseisms from the sea floor (Webb and Cox, 1986).

The Pierson–Moskowitz frequency spectrum is of the form

$$H(\omega) = \alpha g^2 \omega^{-5} \exp[-\beta(\omega_0/\omega)^4], \tag{9}$$

where $\beta \approx 0.74$ is a constant and $\omega_0 = g/U$, where U is the wind speed at a height of 19.5 m. Recent work has suggested an ω^{-4} dependence for the high-frequency tail may be more accurate (Donelan *et al.*, 1985). The exact form of the wave-height frequency spectrum is not crucial to this discussion of microseisms. The two important ingredients are a power law dependence in frequency at high frequencies with a saturated shape mostly independent of wind speed, and a precipitous drop in spectral levels at frequencies below a well-defined cut-off frequency (Fig. 2).

Some model of the directional spectrum of the ocean wave field is required to complete the calculation. Since the generation of microseisms depends on waves traveling in opposing directions the shape of the directional spectrum is crucial. Most acoustic modelers have used a directional dependence of the form

$$G(\theta) = L(q) \cos^q(\theta/2), \tag{10}$$

where q depends on frequency and describes the "beamwidth" of the directional spectrum. The factor L is a normalization parameter. Ocean observations can be fit with q values that vary from about 6 at wave periods near the ocean wave cutoff to small values at higher frequencies, reflecting a change in the spectrum from waves dominated by the wind direction at long periods to a broadly distributed wave field at higher frequencies (Tyler *et al.*, 1974). Present measurement techniques poorly constrain the shape of the directional spectrum outside of a narrow range of azimuths associated with the largest waves that propagate with the wind ($\theta = 0$). However, following virtually all the recent work on microseisms, the directional spectrum will be modeled using Eq. (10) throughout this paper. The specific model for $q(f)$ is shown in Fig. 3(a), and is adapted from the measurements of Tyler *et al.* (1974). The model is scaled by the frequency of the spectral peak ω_0, so that the dependence of beam parameter on frequency varies with the wind velocity.

The dependence of the microseism frequency spectra [Eqs. (6) and (8)] on the directional spectrum of the ocean waves can be shown to be

$$\begin{aligned} I(q) &= \int G(\theta) G(\theta + \pi) d\theta \\ &= \int L^2(q) \cos^q(\theta) \cos^q(\theta + \pi) d\theta. \end{aligned} \tag{11}$$

The effect of the variation of beamwidth with frequency in the model is to reduce the efficiency of microseism generation by about 10 dB from 5 to 0.1 Hz [Fig. 3(b)]. There are

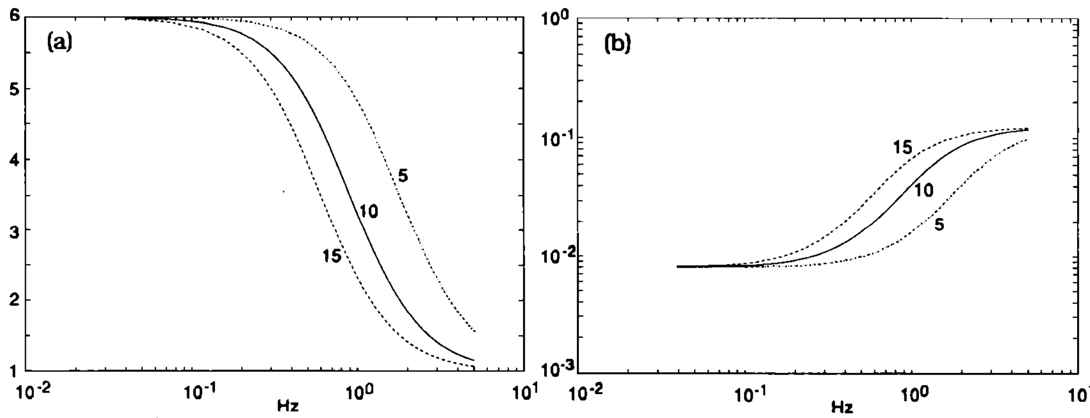

FIG. 3. (a) Model for the directional spectrum of ocean waves at wind velocities of 5, 10, and 15 m/s. The beam parameter q as as function of frequency in a model of the form $\cos^q(\theta)L(q)$ is shown. (b) The dependence of the microseism spectrum on the directional spectrum from [Eq. (11)] as a function of frequency for the three models shown in (a).

wnloaded 30 Jul 2011 to 134.246.166.168. Redistribution subject to ASA license or copyright; see http://asadl.org/journals/doc/ASALIB-home/info/terms

no measurements of sufficient accuracy to constrain the integral over direction in Eq. (11) with any certainty. It is often difficult or impossible to resolve small cross-wind and up-wind components in an ocean wave field dominated by much larger down-wind directed components. The usual practice in ocean wave studies is to assume the up-wind component is zero, and the analysis methods are often designed to minimize the variance in the cross-wind directions (Donelan *et al.*, 1985). Some methods (such as SAR radar) are completely unable to discriminate between components 180° apart [including the Tyler *et al.* (1974) measurements]. It is not likely that measurements of sufficient accuracy to resolve this problem will be made soon.

It is possible that steady winds do not drive waves at sufficiently large angles from the wind direction for the waves to interact to create microseisms, especially at the lowest frequencies in the microseism peak. It may be that it is the variability of the wind direction that determines the directional spectrum. Large shifts in wind direction broaden the wave direction spectrum and generate easily detected, temporary increases in microseism amplitudes (Webb and Cox, 1986; Kibblewhite and Ewans, 1985).

Once waves have propagated outside of the source region, the directional spectrum will depend primarily on the location of the source compared to the point of observation. One differentiates between local wind waves and "swell" from distant sources. The swell component is not expected to contribute to the generation of microseisms except when there is energy in the local wind wave spectrum that can interact with the swell. There is probably a small component of the ocean surface wave field associated with waves reflected from coastlines. It is not known whether the interaction of swell with its reflected component is a significant source of microseisms.

Figure 4 shows predictions for the pressure spectrum deep within an ocean of infinite depth following Eq. (6) for fully developed seas under 5-, 10-, and 15-m/s winds. As

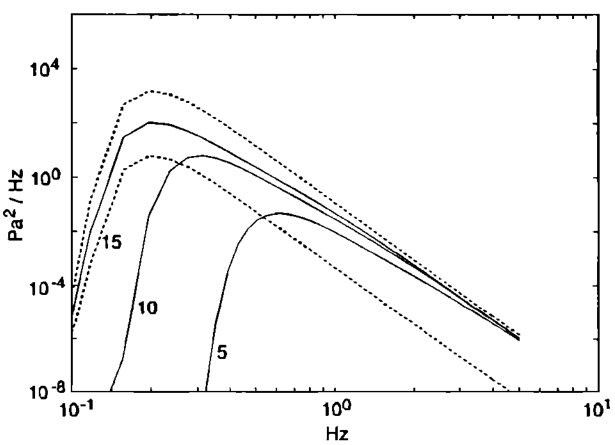

FIG. 4. (Solid line.) The microseism pressure spectrum within an ocean of infinite depth for wind velocities of 5, 10, and 15 m/s under ocean wave spectra as shown in Fig. 2 and directional spectra as shown in Fig. 3. (dashed lines) Microseism pressure spectrum under the ocean wave model spectrum for a wind of 15 m/s and the directional spectrum model with the beam parameter set to either 0 or to 10.

noted by Webb and Cox (1986) and Kibblewhite and Ewans (1985), this spectral form can match seafloor observations of the pressure spectrum to a remarkable extent. To map out the uncertainty in the predicted spectrum associated with the uncertainty in the integral in Eq. (6), the results for directional wave models with the q set to both 0 (an isotropic spectrum) and to 10 (a very narrow spectrum) at a wind velocity of 15 m/s are shown dashed on the figure. Under veering and unsteady winds the directional spectrum will tend toward the isotropic case, and the spectrum will move more toward the upper estimate.

The microseism spectrum is closer to the upper estimate at higher frequencies for which the ocean wave spectrum is more isotropic under steady winds. A changing wind direction should therefore more greatly effect the lower frequencies in the microseism band since the ocean wave directional spectrum will be more profoundly effected. The variability of microseisms is expected to be less at higher frequencies under saturation conditions since the spectrum at higher frequencies will vary less with variations in wind direction. The work of McCreary and Duennebier (1991) using a long record of ambient noise near Wake Island in the Northeast trade winds, seems to demonstrate this prediction. They found less than 5-dB variation in spectral levels at frequencies above 1 Hz for wind sufficient to establish the saturated microseism spectrum, with much greater variability at lower frequencies.

II. RADIATIVE BALANCE EQUATION

Elastic wave velocities increase rapidly within the shallow oceanic crust establishing an efficient waveguide for waves with wavelengths that are comparable to the ocean depth. The microseism signal detected at a point on the seafloor is composed of two parts, one a nonresonant, local component that involves waves of a broad range of wavelengths at a given frequency and the second a component associated with the bound modes of the ocean-seafloor waveguide. This section describes calculations of the modal component of the microseism wavefield.

The most common description of the microseism wavefield is a power spectrum in frequency of the pressure fluctuations or seafloor displacements measured at a point. A more complete description is the wave number and frequency spectrum. It is only very recently that experiments have been devised to measure the wave number and frequency spectra of microseisms at the seafloor (Webb, 1990, 1991; Schreiner and Dorman, 1990).

The wave field within an ocean-seafloor waveguide composed of a vertically stratified stack of plane layers can include both vertically polarized (*P-SV* or Rayleigh mode) and horizontally polarized (*SH* or Love mode) components. Excitation at the sea surface can not directly generate *SH* polarized modes. While scattering by topography at or below the seafloor may couple energy into the *SH* modes, this component is ignored. Each mode has an unique dispersion relation, and so the wave-number spectrum for each mode can be described as a directional spectra $a_n(\theta,\omega)$. The displacements and stresses at a point within the ocean or below

wnloaded 30 Jul 2011 to 134.246.166.168. Redistribution subject to ASA license or copyright; see http://asadl.org/journals/doc/ASALIB-home/info/terms.

the seafloor can be described as a sum over the direction and frequency spectra of the modes. For example, the vertical displacement $w(t)$ can be written as

$$w(\mathbf{x},z,t) = \sum_n \int \int a_n(\theta,\omega) w_n(z) e^{i(\mathbf{k}\cdot\mathbf{x} - \omega t)}\, d\omega\, d\theta, \tag{12}$$

where $\mathbf{k}_n = \omega/c_n\ [\cos(\theta), \sin(\theta)]$ is the vector horizontal wave number of the mode, c_n is the phase velocity, $\mathbf{x}$ is the vector horizontal coordinate, and z is the depth. The eigenfunctions $w_n(z)$ describe the dependence with depth of the vertical displacement in each mode.

Typically, we are interested in a statistical description of the wave field. The kinetic energy density spectrum associated with waves of frequency ω propagating in direction θ for each mode n can be expressed in terms of the normalized direction and frequency spectrum:

$$E_n(\theta,\omega) = A_n \omega^2 I_{1n}, \tag{13}$$

where

$$A_n = \langle |a_n|^2 \rangle$$

are the power spectra of the normalized mode amplitudes and

$$I_1 = \frac{1}{2} \int \rho(u^2 + w^2) dz$$

is an integral over depth of the square of the vertical and horizontal displacements associated with each mode. The integral is defined this way to follow the notation of Aki and Richards (1980). The normalized kinetic energy density is just ω^2 times this integral.

Given the energy spectrum for each mode and hence the power spectra of mode amplitudes, the power spectrum of displacement or pressure at a depth z can be calculated. The vertical displacement frequency spectrum is

$$W(\omega) = \sum_n \int w_n^2(z) A_n(\omega,\theta) d\theta. \tag{14}$$

and the spectrum of pressure fluctuations is

$$P(\omega) = \sum_n \int p_n^2(z) A_n(\omega,\theta) d\theta. \tag{15}$$

where the p_n and w_n are the eigenfunctions in pressure and displacement describing the vertical dependence of each mode. The power spectra of horizontal displacement along two orthogonal horizontal directions (x,y) are, similarly,

$$\begin{aligned} U_x(\omega) &= \sum_n \int u_n^2(z) A_n(\omega,\theta) \cos^2(\theta) d\theta, \\ U_y(\omega) &= \sum_n \int u_n^2(z) A_n(\omega,\theta) \sin^2(\theta) d\theta. \end{aligned} \tag{16}$$

The next step is to allow the energy density spectrum of each mode to be a slowly varying function of location and time $E_n = E_n(\omega,\theta;\mathbf{x},t)$. The spectrum is expected to vary on time and distance scales comparable to ocean weather systems. The spectral balance (radiative transfer) equation for each mode is

$$\frac{\partial E_n}{\partial t} + U_n \cdot \nabla E_n = S_n - D_n + T_n. \tag{17}$$

This equation describes the conservation of energy following a wave packet at group velocity U_n effected by a source S_n, dissipation D_n and with scattering between modes T_n. The source field is also assumed to be a slowly varying function of position and time. This description of conservation and exchanges of energy within a wave field has been a common component of studies of the evolution of the ocean surface gravity wave field (see for example, Hasselmann *et al.*, 1973).

This paper follows the ideas in Hasselmann's (1963) paper on the generation of microseisms. Hasselmann was concerned with estimating the microseism wave field generated by storms at sea as detected by seismometers on land. A finite source region (a single storm) S, is shown in Fig. 5. The source represents a region where ocean waves from a broad set of directions are present, so that wave–wave interactions can transfer energy from ocean waves to elastic waves. To estimate the energy propagating toward a site outside of the source region from the direction θ one projects backward along the ray azimuth through the source region. Beyond the storm the energy E is zero. The energy as a wave packet emerges from the storm can be calculated by integrating the effect of the source along the ray path under the storm using the radiative transfer equation. If the source intensity is constant, the energy grows linearly with time or distance along the ray until effected by dissipation.

The remoteness of site "A" in Fig. 5 from the source region is a good model for microseisms on land, and in the ocean at the lowest frequencies in the microseism peak. Only large (and, hence, rare and usually distant) storms will generate ocean waves of sufficient period to generate the lowest frequency microseisms. The seafloor is different from land in that one is nearly always in the generation region (site "B", Fig. 5) for short period microseisms. From this figure, one can see that the microseism wave energy detected propagating in any direction will depend on the extent of the source region in the direction from which the waves originate, so that measurements obtained at the edge of a stormy region

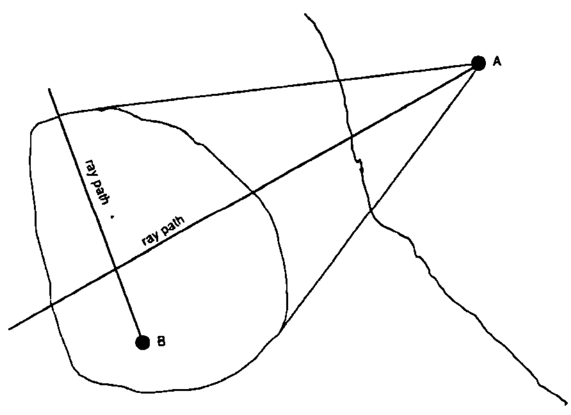

FIG. 5. A sketch of two ray paths of propagating seismoacoustic waves from under a single microseism source region to a site on land ("A") and to a site within the source region ("B").

Downloaded 30 Jul 2011 to 134.246.166.168. Redistribution subject to ASA license or copyright; see http://asadl.org/journals/doc/ASALIB-home/info/terms

should show most of the microseism energy propagating from the direction of the center of the storm.

There are broad regions of the surface of the ocean (such as under the trade winds) which experience at least moderate winds virtually all of the time. These winds in turn generate fully developed seas of a few meters height with wave periods of 10 s or longer. Since microseisms are generated by ocean waves at twice the period, microseisms at frequencies greater than about 0.2 Hz will be excited by a source which extends over huge regions of the ocean. In the absence of attenuation, one would expect the amplitude of microseisms at these frequencies to become very large, as energy is trapped within the waveguide. This is not what is observed, rather the microseism spectrum appears to reach a "saturated" spectrum quickly so that the power spectrum of displacement or pressure looks very nearly the same everywhere on the deep ocean floor.

There are three ways by which the amplitude of the microseisms might be limited. (1) If the source region is of finite extent, then the energy put into the microseisms in the source region is balanced by radiation out of the source region. (2) It is possible that the amplitude of the microseisms might grow to the extent that transfer of energy from surface gravity waves into elastic waves may become balanced by a transfer of energy back into surface gravity waves through a second set of interactions. Microseism displacements appear to be too small by many orders of magnitude for this to be the case. (3) The energy put into microseisms is balanced by dissipation. Included in this mechanism is dissipation that results from scattering into different modes including body waves and subsequent dissipation. Obviously, on a global average, dissipation must eventually always balance excitation. However, what is more interesting, is that for any source that extends over a large region, the dissipation averaged over the region must balance excitation in the region, and in a large uniform region, the local dissipation must balance the local excitation. Thus if one can predict both the excitation and dissipation of the modes, one can predict the amplitude of the microseisms as a function of frequency and as a function of the local surface gravity wave field and the structure of the seafloor.

In the case of a steady, uniform source region of infinite extent the energy spectrum must also be uniform. The radiative transfer equation [Eq. (17)] for each mode reduces to

$$\frac{DE_n}{Dt} = 0 = S_n - D_n + T_n. \tag{18}$$

The dissipation in each mode is related to the mode "Q"

$$D_n(\omega,\theta) = (\omega/Q_n)E_n(\omega,\theta) \tag{19}$$

reflecting the fraction of energy lost per radian.

The source region is modeled as a large uniform region, but within this region there may be small scale heterogeneities in structure that scatter energy between modes. If the density of these scatterers is a slowly varying function then the scattering between modes can be written in terms of scattering coefficients M_{nm}, which are functions of the directions of propagation of pairs of modes. If the scattering heterogeneities are isotropic, then the scattering depends only on the difference in propagation directions $\theta - \phi$. The total scattering in a mode T_n depends on the sum of scattering out of and into the mode:

$$T_n(\omega,\theta) = E_n(\omega,\theta) \sum_m \int_0^{2\pi} M_{nm}(\omega,\theta-\phi)d\phi + \sum_m \int_0^{2\pi} M_{mn}(\omega,\theta-\phi)E_m(\omega,\phi)d\phi. \tag{20}$$

The first term can be written as an extrinsic attenuation (Kennett, 1990):

$$b_n = \sum_m \int_0^{2\pi} M_{nm}(\omega,\theta-\phi)d\phi$$

so that the total attenuation can be written as a sum of the intrinsic and extrinsic attenuation:

$$D_n(\omega,\theta) = \left(\frac{\omega}{Q_n} - b_n\right)E_n(\omega,\theta). \tag{21}$$

Calculating the b_n's is far beyond the range of this paper. The second term in Eq. (20) is equally difficult, however, in general, it appears that usually a single mode may dominate the microseism wave field at any particular frequency so that the transfer of energy out of the dominate mode will be the primary energy exchange.

Kennett (1990) provides an analysis following the techniques of Kohler and Papanicolaou (1977) of the 2-D case of attenuation due to scattering by random inhomogeneities in a wave guide for elastic waves. Equations (17) and (20) can be combined to define a set of "coupled power equations" outside of the source region:

$$U\frac{\partial E_n}{\partial x} = \left(-\frac{\omega}{Q} + b_n\right)E_n + \sum_m H_{mn}E_m, \tag{22}$$

which include both forward and backward scattering. Details of the calculations of the scattering coefficients can be found in Kennett (1990).

Scattering between modes will be ignored in the remainder of this paper, although Schreiner and Dorman (1990) have evoked scattering into short wavelength Stoneley modes to explain the rapid loss of coherence with distance observed between measurements from pairs of sensors separated on the seafloor. Models of scattering from the rough basalt–sediment interface in regions of thin sediment suggest scattering into sediment modes may indeed be important in many regions of the seafloor at frequencies near 1 Hz (Dougherty and Stephens, 1988).

The next section proceeds with the calculation of the excitation function. The source region is assumed to be so large that the source looks the same in every direction so that the energy spectrum is isotropic in direction. We equate the energy being put into each mode by the ocean waves to the dissipation per unit area to determine the energy spectrum:

$$E_n(\omega,\theta) = (Q_n/\omega)S_n(\omega,\theta) \tag{23}$$

An integral over azimuth θ leads to the excitation rate per unit area and the energy density per unit area in each mode:

$$E_n(\omega) = \frac{Q_n}{\omega} S'(\omega) = \frac{Q_n}{\omega} \int S_n(\omega,\theta)d\theta. \tag{24}$$

wnloaded 30 Jul 2011 to 134.246.166.168. Redistribution subject to ASA license or copyright; see http://asadl.org/journals/doc/ASALIB-home/info/terms

The next problem is to calculate the source function for each mode S'_n.

III. CALCULATIONS OF MODE EXCITATION

The microseism excitation is modeled as a distribution of vertical dipoles (a pressure field) at the free surface. The vertical displacement field due to this distributed pressure field $P(x,\omega)$ can be calculated using an integral over the free surface of the Green's function for a vertical point force at the surface times the pressure field. Assuming a Fourier transform in frequency, the displacement at a point described by the horizontal vector $\mathbf{x}$ and depth z is expressed as a sum over modes:

$$w(\mathbf{x},z,\omega) = \sum_n \int G_{pw,n}(\mathbf{x},z,\omega;\mathbf{x}_0,z_0)p(\mathbf{x}_0,\omega)d\mathbf{x}_0. \quad (25)$$

The Green's function in cylindrical coordinates for a vertical point force can be found in Aki and Richards (1980):

$$G_{pw,n}(\mathbf{x},z,\omega;\mathbf{x}_0,z_0) = \frac{iw_n(z)w_n(z_0)}{8c_n U_n I_{1n}} J_0[k_n|\mathbf{x}-\mathbf{x}_0|)], \quad (26)$$

where J_0 is the zeroth-order Bessel function and the w_n are the vertical displacement eigenfunctions. The Green's function can be rewritten as an explicit function of only the relative position $|\mathbf{x}-\mathbf{x}_0|$ and evaluated at the free surface $z_0=0$.

The rate of work done by the pressure field at the free surface on a mode is the time average of the product of the vertical velocity in the mode at the free surface and the pressure acting at the surface (the dot product of traction and particle velocity):

$$\begin{aligned} W(\mathbf{x},\omega) &= \langle -i\omega w(\mathbf{x},0,\omega)p^*(\mathbf{x},\omega)\rangle \\ &= -i\omega \sum_n \int G_{pw,n}(|\mathbf{x}-\mathbf{x}_0|,0,\omega) \\ &\quad \times \langle p(\mathbf{x}_0,\omega)p^*(\mathbf{x},\omega)\rangle d\mathbf{x}_0. \end{aligned} \quad (27)$$

The quantity in angle brackets is the autocorrelation function of the surface pressure field [Eq. (2)]. As noted earlier, a delta function can be used to approximate this function since the scale of the correlation is very small compared to acoustic wavelengths [Eq. (3)]. Equation (27) evaluates trivially

$$\begin{aligned} W(\omega) &= \sum_n -i\omega C(\omega) \int_0^\infty \int_0^{2\pi} G_{pw,n}(|\mathbf{x}-\mathbf{x}_0|,\omega) \\ &\quad \times \delta(|\mathbf{x}-\mathbf{x}_0|)d\mathbf{x}\,d\theta, \end{aligned} \quad (28)$$

$$W(\omega) = \sum_n -i\omega G_{pw,n}(0,\omega)C(\omega).$$

The source function for each mode is then

$$S'_n(\omega) = \frac{2\pi\omega w_n^2(0)}{8c_n U_n I_{1n}} C(\omega). \quad (29)$$

Equating the source and dissipation terms determines the mode amplitude power spectra:

$$A_n(\omega) = \frac{\pi w_n^2(0)Q_n}{4\omega^2 c_n U_n I_{1n}^2} C(\omega). \quad (30)$$

The equilibrium amplitude spectra are linear with the mode Q, and inversely related to the energy density transport rate $U\omega^2 I_n$ normalized by the vertical displacement at the free surface. Functions for each mode for the vertical displacement and pressure at the seabed ($z=h$) can be defined from Eqs. (14), (15), and (30) for which the local dissipation and excitation are equal:

$$\begin{aligned} V_n(\omega,h) &= w_n^2(h)\frac{\pi w_n^2(0)Q_n}{4\omega^2 c_n U_n I_{1n}^2}, \\ P_n(\omega,h) &= p_n^2(h)\frac{\pi w_n^2(0)Q_n}{4\omega^2 c_n U_n I_{1n}^2}. \end{aligned} \quad (31)$$

A sum over these functions yields transfer functions between the source spectrum and the seafloor displacement (T_w) and pressure (T_p) spectra, which will be called the equilibrium transfer functions:

$$\begin{aligned} W(\omega,h) &= C(\omega)\sum_n V_n = C(\omega)T_w(\omega,h), \\ P(\omega,h) &= C(\omega)\sum_n P_n = C(\omega)T_p(\omega,h). \end{aligned} \quad (32)$$

IV. CALCULATIONS OF MODE EXCITATION AND DISSIPATION IN REALISTIC EARTH MODELS

The earth models considered here consist of a vertical stack of laterally homogeneous layers of differing density, compressional, and shear velocity. The propagator matrix method combined with the method of minor vectors is a computationally stable method to determine the normal modes in this type of model (Woodhouse, 1980). We use an implementation written by Gomberg and Masters (1987). Figure 6(a) displays the phase velocity as a function of frequency for the first 30 modes in a model representing thinly sedimented oceanic crust. This model [Fig. 7(a)] is from Adair (1985) based on the work of Kim *et al.* (1987) and Shearer and Orcutt (1985), from a site in the central Pacific. The model will be called the "Pacific model" in this paper. There are three related types of *P-SV* polarized modes in the

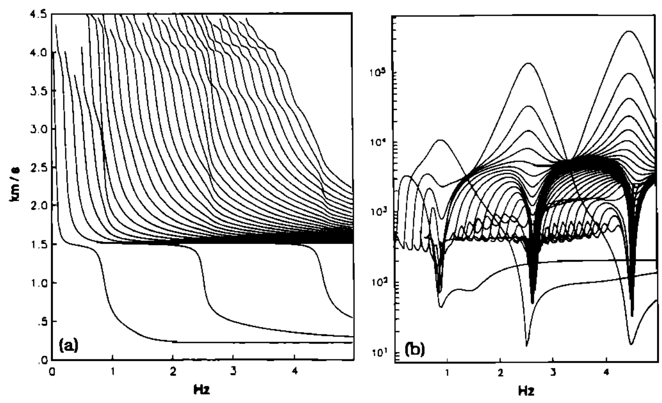

FIG. 6. (a) Phase velocity versus frequency for the first thirty modes in the Pacific model (Fig. 7). (b) The "Q's" as a function of frequency associated with the modes shown in (a).

Downloaded 30 Jul 2011 to 134.246.166.168. Redistribution subject to ASA license or copyright; see http://asadl.org/journals/doc/ASALIB-home/info/terms

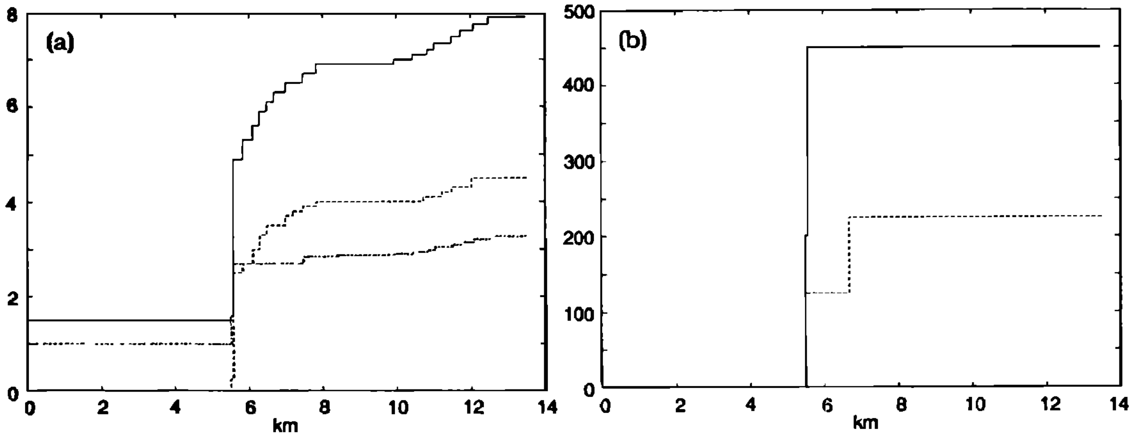

FIG. 7. The "Pacific model": (a) Compressional velocity (solid line, km/s), shear velocity (heavy dashed line, km/s) and density (light dashed line, gm/cm^3) versus depth. (b) Compressional wave (solid line) and shear wave (dashed line) "Q's" as a function of depth (km). The compressional wave Q is set infinite in the 5.5-km-deep ocean.

oceanic waveguide, corresponding to (1) Rayleigh waves in the crust and mantle, (2) primarily acoustic modes in the ocean, and (3) Stoneley modes associated with the thin layer of low shear velocity sediment (Panza, 1985). A mode will fit generally into one of these categories depending on frequency, although for the most part, some energy is shared between the mantle, crust, sediment, and ocean in every mode and at all frequencies. The modes that look mostly "acoustic" will propagate with the least attenuation, while modes with energy trapped in the sediment, rapidly attenuate.

The mode Q's can be derived from estimates of the Q's for propagation of both shear Q_β and compressional waves Q_α within each layer of the model. The mode Q's are a weighted integral over the layers:

$$Q^{-1}=\frac{1}{4c^2I_1}\left\{\int_0^\infty \left[\left(ku+\frac{dw}{dz}\right)^2(\lambda+2\mu)\right]2Q_\alpha^{-1} + \left[\left(kw-\frac{du}{dz}\right)^2-4ku\frac{dw}{dz}\right]2\mu Q_\beta^{-1}\,dz\right\}. \tag{33}$$

Here, w and u refer to vertical and horizontal displacement eigenfunctions and λ and μ are Lame coefficients (Aki and Richards, 1980). The index n referring to the particular mode is assumed in this equation. The Q's derived from this equation are "temporal Q's" referring to the fraction of energy lost each wave period. This Q differs from a "spatial Q" that is weighted by the ratio of the group velocity to the phase velocity to describe the energy lost per wavelength traveled.

The attenuation coefficients (or Q's) of shear and compressional waves are less well known than the compressional and shear wave velocities. Wave attenuation estimates are obtained as part of full wave modeling of refraction data and from Rayleigh and Love wave propagation measurements. The amplitude spectra are linear in mode Q, so uncertainties in layer Q's are directly related to uncertainties in the microseism spectrum. The microseism spectrum ranges over more than 70 dB across the band from 0.1 to 10 Hz, so uncertainties of 50% in energy associated with errors in Q are nearly invisible on plots of spectra. Figure 7(b) shows estimates of the shear and compressional wave Q's derived from Spudich and Orcutt (1980). Attenuation of compressional waves within the ocean at the frequencies considered here is negligible and the ocean Q is set infinite in the model. Compressional wave and shear wave Q values in the mantle are estimated to be about 450 and 225 leading to mode Q's around 300 for mantle Rayleigh waves.

The attenuation within sediments is much higher than in the rock or the ocean. Sauter (1987) measured Q values near 40 in the upper 50 m of a muddy seafloor. Recent work suggests the attenuation in very young oceanic crust in seismic layer "2*A*" can also be very large ($Q\approx 30$, Wilcock *et al.*, 1991). In the calculations shown here, the high attenuation in a thin layer of sediments does not greatly effect the attenuation of modes which contribute to the signal seen at the seafloor since modes with significant energy in the sediment layer tend to be poorly excited by a source at the sea surface. The high attenuation does become important when considering scattering into sediment modes at the sediment–rock boundary, then the high attenuation will tend to "soak up" any energy scattered into these modes. Figure 6(b) shows the mode Q's which range from 10^5 for modes with energy primarily in the ocean to 50 for Stoneley phases. The largest Q values are probably overly large, a result of setting dissipation to zero in the seawater, however these large values do not effect the results shown in this paper. The model also does not include the very large attenuation associated with the upper few meters of sediment so that the Stoneley mode Q's are too large at high frequency. However, these modes are also not an important component of the results.

The modal functions [Eq. (31)] for pressure and displacement are summed to derive the equilibrium transfer functions [Eq. (32)] in Fig. 8(a) and (b). The individual modal functions are complicated, but the sum of these curves yields smoother curves with an approximately power

wnloaded 30 Jul 2011 to 134.246.166.168. Redistribution subject to ASA license or copyright; see http://asadl.org/journals/doc/ASALIB-home/info/terms.

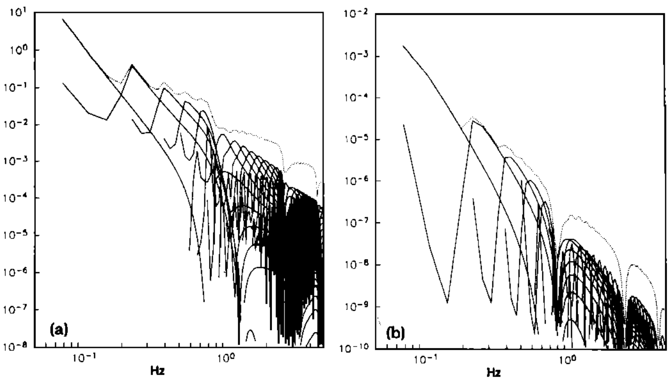

FIG. 8. (Solid lines.) The modal transfer functions of (a) displacement and (b) pressure in the Pacific model. The sum of the modal transfer functions is shown as a dashed line. The transfer functions relate the equilibrium microseism spectrum to the frequency spectrum of the spatial correlation function of the source.

law dependence of about f^{-3} for pressure and f^{-2} for vertical displacement. At low frequencies, one mode usually contributes at least 80% of the variance at any particular frequency. The order of the dominate mode increases with increasing frequency. There are necessarily frequencies when two modes contribute equally. Above 1 Hz, the contributions from several modes may be comparable. The peak values in the modal excitation functions are associated with the parts of dispersion curves when the modes look most like acoustic modes in the ocean with phase velocities between 1.5 and 3 km/s (Fig. 6). The largest value in each excitation function occurs in the "elbow" of the dispersion curve where the phase velocity is near 1.6 km/s and there is a local minimum in the group velocity.

Figure 9 displays the vertical displacement spectrum at the seafloor calculated using the Pacific model in Fig. 7 and the Pierson–Moskowitz model of a fully developed surface gravity wave spectrum at three different wind velocities (Fig. 2). The wind wave directional spectrum is as specified in Eq. (11) and Fig. 3. As noted earlier, the directional spectrum is a crucial component of the calculations that is poorly constrained by measurements. In Fig. 9, stronger winds generate lower frequency ocean waves which in turn generate lower frequency microseisms. At high frequencies the microseism spectrum is independent of the wind velocity if the velocity is above some critical value. The vertical displacement spectrum model has a power law dependence on frequency with a slope of about 100 dB/decade. The spectrum decreases precipitously below the cutoff frequency. An example of a displacement spectrum measured at the seafloor near DSDP drilling site 469 is shown is also shown in Fig. 9 (data from Schreiner and Dorman, 1990). The model spectra exceed the data at this site by as much as 10 dB over part of the microseism band, but the general shape and slope is correct. As noted in Fig. 4, the uncertainties associated with the knowledge of the directional spectrum of the ocean wave source are of comparable magnitude. The spectrum may not be saturated across the entire microseism band, and teleseismic energy probably controls the spectrum near 0.1 Hz.

The model for the pressure spectrum is compared with measurements of the pressure spectrum from three sites in eastern Pacific in Fig. 10. The slope of the forward face of the pressure spectrum is about 70 dB/decade. This model spectrum is the sum of the resonant component from Eq. (32) and the nonresonant component inferred from Eq. (6). The

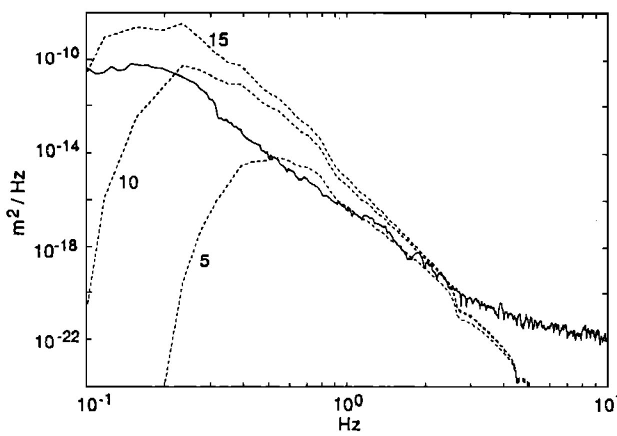

FIG. 9. (Solid line.) Displacement spectrum from the seafloor in the eastern Pacific. (dashed lines) Model displacement spectra for the Pacific model at wind velocities of 5, 10, and 15 m/s assuming the ocean wave model in Figs. 2 and 3 and the transfer function shown in Fig. 8.

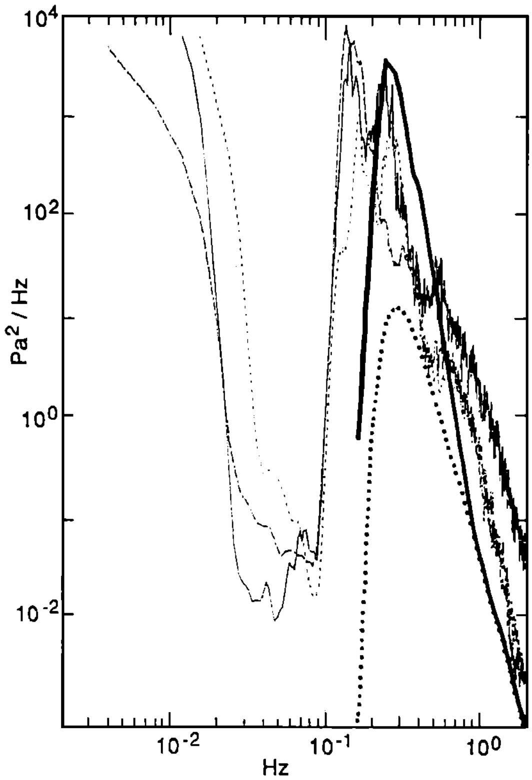

FIG. 10. (Thin solid and dashed lines.) Three pressure spectra from sites in the eastern Pacific. The local wind-wave microseism peak varies from 0.2 to 0.5 Hz in these three spectra. (Heavy solid line.) Model pressure spectrum for the Pacific model for a wind velocity of 10 m/s. (Dotted line.) A model for the nonresonant component of the pressure spectrum.

Downloaded 30 Jul 2011 to 134.246.166.168. Redistribution subject to ASA license or copyright; see http://asadl.org/journals/doc/ASALIB-home/info/terms

resonant component associated with the trapped modes is considerably larger than the nonresonant component (dotted line, Fig. 10) across most of the microseism band, but falls slightly below the nonresonant component above 0.8 Hz. The pressure spectra shown in Fig. 10 are combinations of both local wind driven peaks ranging from 0.2 to 0.6 Hz and a (probably) teleseismic peak near 0.13 Hz. This teleseismic peak shows an evolution with time toward higher frequency suggesting normal dispersion of ocean waves from a distant storm (Webb and Cox, 1986).

The apparent "gain" associated with trapping of energy in modes of the waveguide can be estimated by dividing the total result in Fig. 10 by the result from Eq. (6). The apparent gain in pressure is as high as 43 dB near 0.15 Hz [Fig. 11(a)], considerably larger than the results of Schmidt and Kuperman (1988) for deep water. The apparent gain in vertical displacement of the seafloor using the results in Fig. 10 and Eq. (8) exceeds 20 dB at 0.15 Hz [Fig. 11(b)] also larger than the Schmidt and Kuperman results. The discrepancy between the two sets of calculations is primarily the result of different models of attenuation. The compressional and shear wave Q's in the sediments and rock in Fig. 7 correspond to attenuation coefficients of between 0.01 and 0.03 dB/λ, about one-tenth of the values used in the Schmidt and Kuperman paper, hence a 10-dB difference in model predictions.

The dependence of the seafloor pressure spectrum on the structure beneath the seafloor seems to be greater than the dependence of the vertical displacement spectrum on structure. The displacement spectrum predicted from a model with a deep layer of sediments [Fig. 12(a)], is only about 3 dB quieter than the spectrum derived from the thinly sedimented model whereas the pressure spectra differ by up to 15 dB with the difference greatest near 0.25 Hz [Fig. 12(b)]. The dispersion curves for the two earth models are quite different as are the modal Q's (Figs. 6 and 14). One of the original goals of this work was to understand why measurements of the microseism pressure spectra from a site in the western Atlantic were always less energetic than spectra from sites in the eastern Pacific. The model with the deep

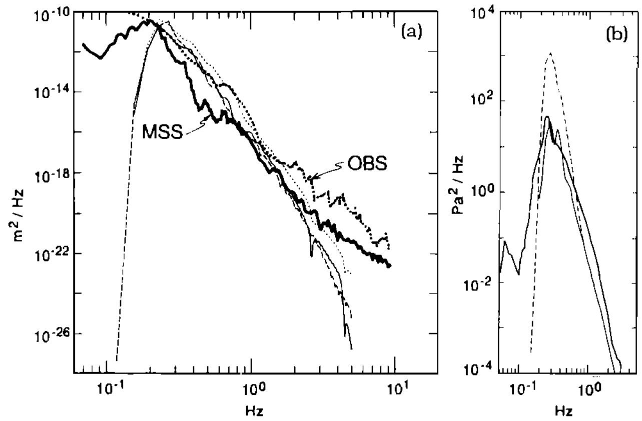

FIG. 12. (a) Measurements of the displacement spectra from a borehole at a depth of 509 m (heavy solid line), and the seafloor (heavy dotted line). Also shown are models for the displacement at the seafloor (light dashed line), and in the borehole (light solid line) in the Pacific model and at the seafloor in the Atlantic model (light broken line). (b) Seafloor pressure spectrum from a site in the western Atlantic (heavy solid line), and model pressure spectra for the seafloor in the Atlantic (light solid line) and Pacific models (dashed line).

layer of sediment (Fig. 13) will be called the "Atlantic" model although representing only the edges of the basin with significant terrigenous sediment. An example of the pressure spectrum from a site on the seafloor in the Western Atlantic resembles closely predictions from this model [Fig. 12(b)]. A deep layer of sediments does significantly attenuate the pressure spectrum seen at the seafloor and apparently explains the differences between eastern Pacific and western North Atlantic sites. Microseism spectra in the two oceans should also differ because of differences in wave climatology.

The predicted pressure spectrum in the Atlantic model is smaller than the predicted spectrum for the Pacific, because the typical mode Q's for the "acoustic-like" modes with phase velocities near 1.5 km/s are on the order of 90 in the Atlantic model and 3000 in the Pacific model, representing the difference in attenuation between models with deep

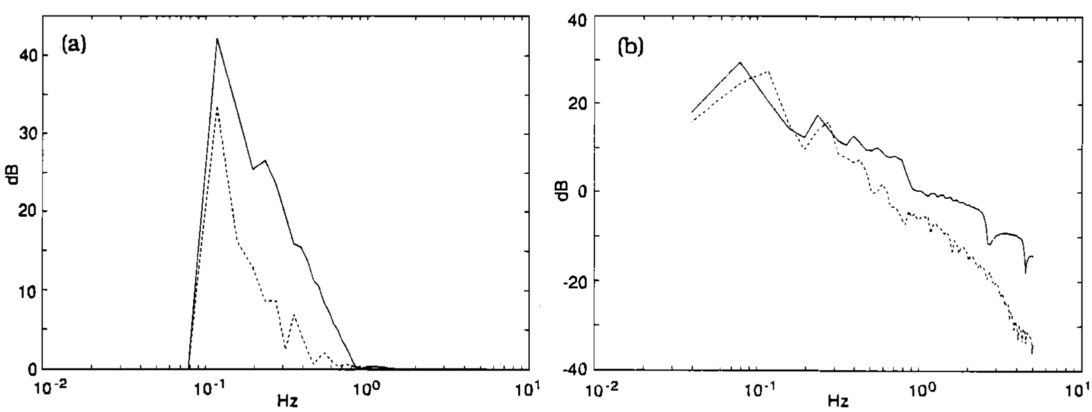

FIG. 11. Apparent gains in dB in pressure (a) and displacement (b) in the Pacific (solid line) and Atlantic (dashed line) models. The figure compares the microseisms in the ocean-seafloor waveguide under an extended source region to the result for a model of microseisms in an ocean of infinite depth.

wnloaded 30 Jul 2011 to 134.246.166.168. Redistribution subject to ASA license or copyright; see http://asadl.org/journals/doc/ASALIB-home/info/terms

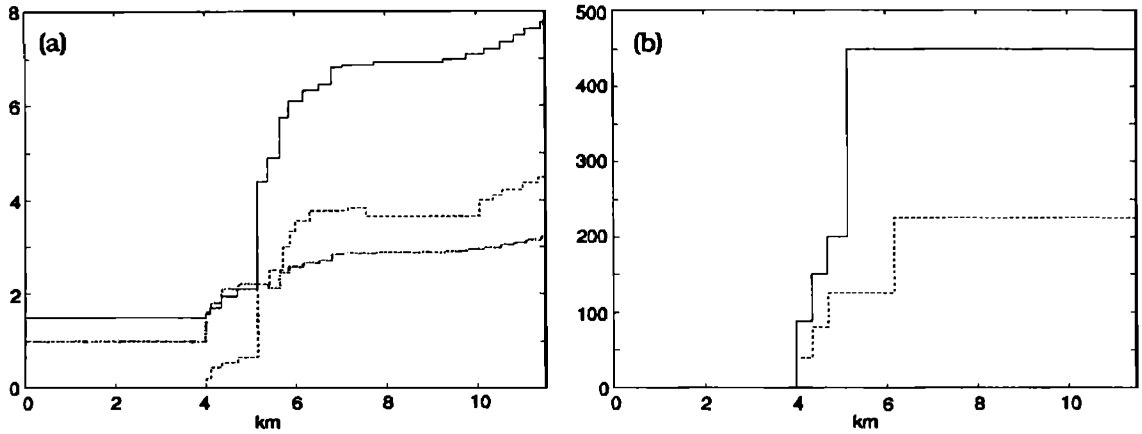

FIG. 13. The "Atlantic model": (a) Compressional velocity (solid line, km/s), shear velocity (heavy dashed line, km/s) and density (light dashed line, gm/cm^3) versus depth (in km). (b) Compressional wave (solid line) and shear wave (dashed line) "Q's" as a function of depth (km). The compressional wave Q is set infinite in the 4-km-deep ocean.

and thin layers of sediments (Figs. 6 and 14). The vertical displacement spectra in the two models are more similar than the pressure spectra because the reduction in microseism energy associated with greater attenuation in the sediments is partly countered by larger vertical displacements at the seafloor associated with lower shear strength in the sediments.

V. BOREHOLE SEISMIC MEASUREMENTS

There has been a debate about the utility of burying seismometers within the crust to improve the signal to noise on high phase velocity components (body wave phases). The model predicts the vertical displacement spectrum for a seismometer at depth within a borehole should be less energetic than the spectrum at the surface by about 10 dB, a consequence of more rigid rock at depth [Fig. 12(a)]. The vertical scales of modes excited from the sea surface are large, so in the model used for these predictions, shallow burial is not greatly advantageous. If strong scattering into short wavelength components at the seafloor occurs, then the spectral level at the seafloor would increase with a lesser effect on the borehole measurements. The net effect of scattering is to reduce the total energy transport in microseisms (integrated over depth) because of the greater attenuation, but the spectral level near the seafloor should increase because of trapping of energy near the interface.

Vertical displacement spectra from the seafloor near DSDP borehole 395A in the western Pacific and at depth, 609 m below the seafloor differ by from 10 to 20 dB (Adair *et al.*, 1984). The model spectrum (Pacific model) matches the borehole measurements within 10 dB over most of the microseism band. The model underpredicts the displacement measurements at the ocean floor by 10 to 15 dB over most of the band [Fig. 12(a)]. Adair *et al.* (1984) have argued that the large difference in spectral amplitudes between down hole and surface measurements at this site is the result of significant scattering into short vertical wavelength components. Dorman and Schreiner (1990) have also argued for significant scattering into Stoneley mode phases based on observations of the correlation scale between instruments separated horizontally on the seafloor.

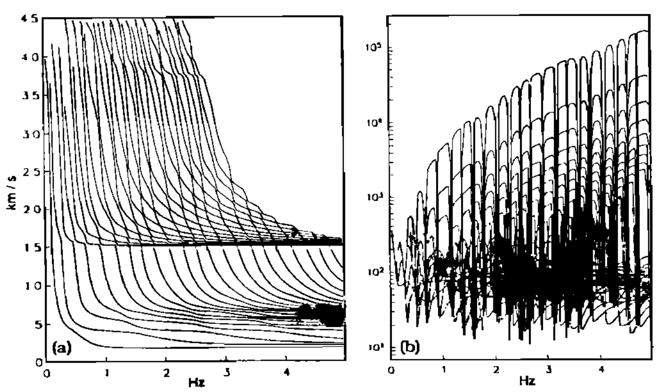

FIG. 14. (a) Phase velocity versus frequency for the first thirty modes in the Atlantic model (Fig. 13). (b) The "Q's" for the modes shown in (a).

VI. SHALLOW WATER

The character of microseisms is very different in shallow water. The water depth determines the "cut-off" frequencies of ocean acoustic modes and fewer and fewer modes look like ocean acoustic modes as the water depth is reduced. The microseism energy is therefore carried by the Rayleigh wave modes. The amplitude of the microseism peak in equilibrium pressure spectrum calculations is 40 dB less in 500-m water depth compared to deep water [Fig. 15(a)]. In contrast, the equilibrium displacement spectrum is reduced by at most 20 dB from deep water to 500-m depth [Fig. 15(b)]. In shallow water, the wavelength of acoustic waves at microseism frequencies becomes large compared to the water depth so that the pressure signal associated with the normal modes is reduced at the seafloor because of the proximity of the free surface. Teleseismic phases are therefore difficult to detect with pressure gauges. The entire microseism signal in pressure is local, and a direct measure of the forcing overhead

wnloaded 30 Jul 2011 to 134.246.166.168. Redistribution subject to ASA license or copyright; see http://asadl.org/journals/doc/ASALIB-home/info/terms.

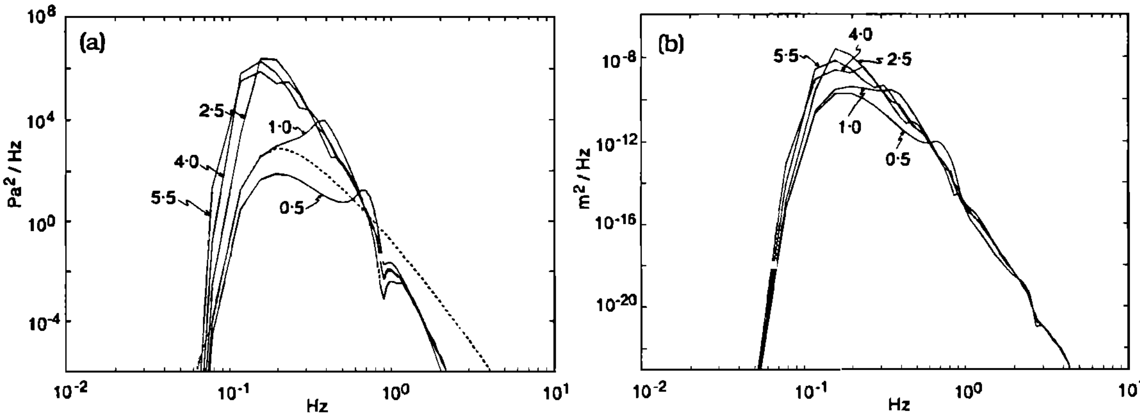

FIG. 15. (a) The equilibrium microseism model results for (a) pressure and (b) displacement spectra in water of depths ranging from 0.5 to 5.5 km using the Pacific model. The dashed line in (a) is the result for an ocean of infinite depth.

(Kibblewhite and Wu, 1991; Kibblewhite and Ewans, 1985). Measurements of the pressure spectrum from 500-m depth from the coast of Oregon show greater variability from day to day than is ever seen in deep water measurements (Fig. 16). In the first day of measurements under calm winds, the pressure spectrum is under 1 Pa^2/Hz over the entire microseism band from 0.1 to 0.5 Hz. This is smaller by 20 dB than any measurement of the microseism peak from deep water (except for the Arctic ocean seafloor). The robustness of the amplitude of the infragravity wave energy below 0.04 Hz confirms the instrumentation is functional. During the second day of measurements, increasing wind generates a local wind wave peak that evolves toward lower frequency with time. The frequency of this peak falls to 0.18 Hz at the end of data series and the amplitude of the peak is comparable to that expected for the "nonresonant" component [10^3 Pa^2/Hz, Fig. 15(a)].

The most important result of the calculations shown here is that in deep water, large changes in structure below the seafloor leads to only small changes in the results, particularly in the displacement spectrum. The theory provides an explanation for the remarkable uniformity in the amplitude and shape of the microseism peak seen at the seafloor. The uniformity of spectral amplitude seen in deep water is also a consequence of efficient propagation of energy within the ocean-seafloor waveguide as discussed in the next section.

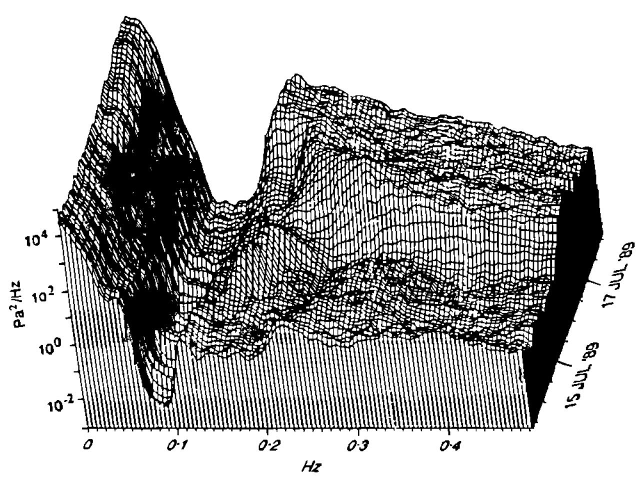

FIG. 16. A series of pressure spectra from the continental rise off of central Oregon, from a water depth of 500 m. The pressure spectrum varies more greatly here than in deep water because the pressure signal from the teleseismic component is reduced in shallow water.

VII. THE APPROACH TO EQUILIBRIUM

The calculations shown so far assume a source region of infinite extent. An important question is how quickly the spectrum evolves to the equilibrium spectrum. The radiative transfer equation for each mode with a source term and a dissipation term can be written as

$$\frac{\partial E_n(\omega,\theta)}{\partial t} + U_n\cdot\nabla E_n = S_n - \frac{\omega}{Q_n} E_n. \tag{34}$$

In a solitary, uniform amplitude, temporally stationary, finite source region, the equation for each mode following a ray along direction θ simplifies to an equation in a single coordinate, the distance along the ray x since the group velocity is independent of location:

$$U_n \frac{\partial E_n}{\partial x} = S_n - \frac{\omega}{Q_n} E_n. \tag{35}$$

If E_n is zero before entering the source region at $x = 0$ the general solution along the ray path for $x > 0$ is

$$E_n(\omega,\theta) = \frac{Q_n}{\omega} S_n \left[1 - \exp\left(\frac{-x\omega}{U_n Q_n}\right)\right]. \tag{36}$$

If the source region is circular, the energy along all rays directed toward the center will be the same. The total energy in a mode at the center is found by integrating over direction, equivalent to multiplying Eq. (36) by 2π. Using this equation, the contributions to the spectrum from each mode in a region of order R in radius can be calculated. Much of the energy is in modes with Q's on the order of 300. Given a typical group velocity of 1.5 km/s, a characteristic length

wnloaded 30 Jul 2011 to 134.246.166.168. Redistribution subject to ASA license or copyright; see http://asadl.org/journals/doc/ASALIB-home/info/terms.

corresponding to a single e-folding at 5-s period is about 2200 km. After one e-folding the spectrum is within 4 dB of the equilibrium spectrum, which for most measurements is indistinguishable from the equilibrium spectrum.

The ratio of the pressure spectra under source regions of 10, 100, or 1000 km in radius to the spectrum in a region of infinite extent is shown in Fig. 17(a). The Q's in the Atlantic model tend to be considerably less than in the Pacific model so the spectrum is closer to equilibrium spectrum in a smaller region. The power in the spectrum in the microseism band is within 15 dB of the fully saturated value within a source region of about 100-km radius in the Pacific and just 20 km in the Atlantic model. The e-folding scale tends to be less at higher frequency, so that saturation is obtained in a smaller region. The spectrum above 0.7 Hz is always within 5 dB of saturation within a source region of only 100 km so the spectrum at these frequencies should appear fully saturated at any site where the wind exceeds about 5 m/s. Typical source regions will usually be 100 to 1000 km in extent so that the energy in microseism peaks near 0.2 Hz will usually lie 3 to 8 dB below the saturated value in the Pacific.

How large must a region of calms be to see a significant reduction in the microseism spectrum below the equilibrium spectrum? The decay of microseism spectrum away from a source region can be estimated by calculating the attenuation of modes with distance;

$$E_n = \frac{Q_n}{\omega} S_n \exp\left(\frac{-x\omega}{U_n Q_n}\right). \tag{37}$$

Again the differences in mode Q's between the Atlantic model and the Pacific model are important. In the Pacific model, the mode Q's at frequencies below 0.6 Hz are sufficiently large that a calm region must exceed several thousand kilometers in scale for the microseism spectrum to fall more than 10 dB below the saturation value [Fig. 17(b)]. These large scale lengths suggest that in the Pacific, it is nearly impossible for the microseism energy to fall much below the saturation value since ocean storms somewhere will be creating microseisms which are seen at any site. The large mode Q's near 0.15 Hz suggest this energy, once established will propagate throughout an ocean basin. The spectrum falls more quickly within a region of calms in the Atlantic model, but there is still some energy at frequencies below 0.3 Hz, which propagates thousands of kilometers [Fig. 17(c)]. The greater attenuation associated with the Atlantic model should permit spectra to deviate greatly from the saturation spectrum in regions of calms at sites for which this model is appropriate. The spectral decay curves for the Atlantic model [Fig. 17(c)] exhibit great variability in attenuation between closely spaced frequencies. The natural variation in earth structure should eliminate most of this complex structure.

VIII. MICROSEISM CLIMATOLOGY

A goal of this work was to understand why microseism spectra from the seafloor at a site in the North Atlantic were less energetic than pressure measurements from the Pacific seafloor. One answer is that the greater attenuation associated with deep layers of sediments reduces the microseism signal [Fig. 12(b)]. A second answer is that the ocean wave climate in the Pacific is almost invariably more energetic than in the western, central North Atlantic. This section discusses the climatology of ocean waves and the resultant microseism climatology as a guideline to predicting low-frequency acoustic noise throughout the ocean basins.

Measurements from the deep seafloor of the Arctic under the icecap provide an estimate of the background microseism spectrum, far from local sources. The ice cover prevents the development of ocean waves eliminating ocean waves as a source of microseisms. Figure 18 shows a spectrum obtained from an instrument on the floor of the Beaufort Sea from March 1990. Microseisms are still evident, but the spectrum is very subdued; 30 to 40 dB quieter than spectra from the Pacific seafloor. The nearest source of microseisms is across Alaska in the Northeast Pacific ocean (Webb and Schultz, 1992).

Elsewhere in the ocean, the microseism spectrum is composed of a local part associated with winds and waves within a few hundred kilometers of the site, and a lower frequency, teleseismic part associated with low-frequency

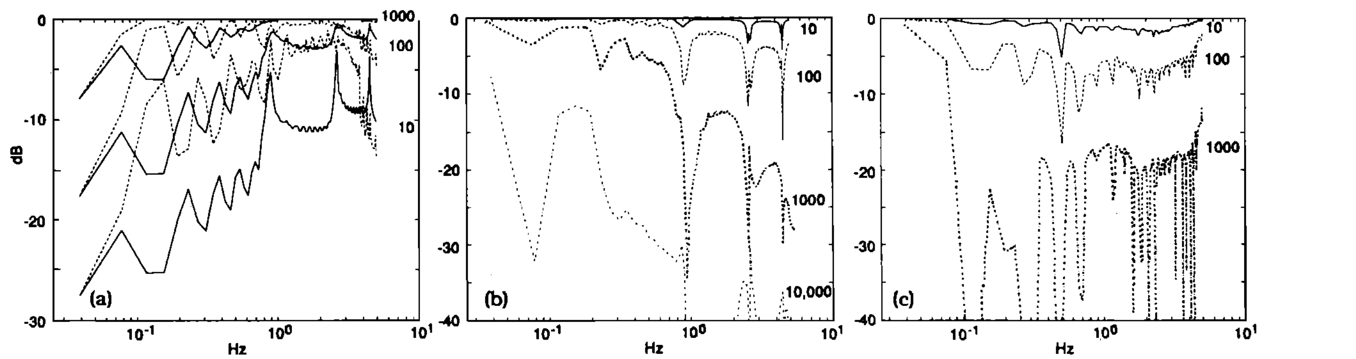

FIG. 17. (a) The ratio of the pressure spectrum in three regions of finite extent (10, 100, and 1000 km in radius) to the "equilibrium spectrum" in a region of infinite extent in the Pacific model (solid lines) and the Atlantic model (dashed lines). (b) The decay of the microseism pressure spectrum into a region without forcing adjacent to a region with a fully excited (equilibrium) microseism spectrum. The ratio of the pressure spectrum at distances of 10, 100, 1000, and 10 000 km into the calm region to the equilibrium spectrum in the source region is shown for the Pacific model. (c) same as (b) except the spectra are derived from the Atlantic model, and the curve at 10000km is not shown.

Downloaded 30 Jul 2011 to 134.246.166.168. Redistribution subject to ASA license or copyright; see http://asadl.org/journals/doc/ASALIB-home/info/terms

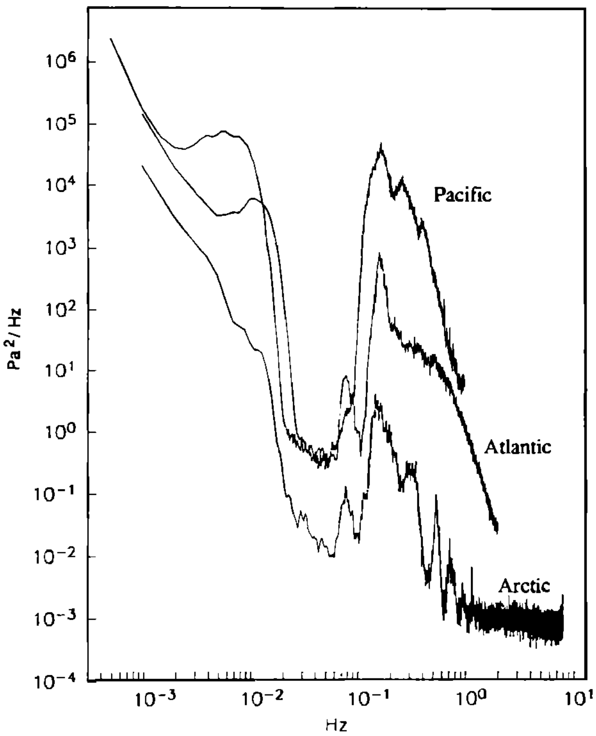

FIG. 18. Pressure spectra from sites on the seafloor in the Pacific, Atlantic, and Arctic oceans.

ocean waves from usually distant and large storms. Figure 2 shows the ocean wave spectrum at wind velocities of 5 and 10 and 15 m/s at a prescribed height (19.8 m). The lowest frequencies in each spectrum are sharply limited. Under a 5-m/s wind, the spectrum approaches the saturated spectrum only for frequencies above about 0.3 Hz, for 10 m/s, the spectrum is saturated to slightly lower frequency (0.15 Hz) and at 15 m/s to 0.1 Hz. After accounting for the frequency doubling associated with the nonlinear microseism spectrum, we see that a wind velocity near 10 m/s is required to significantly excite 0.2-Hz microseisms, but that only 5 m/s is required to excite 0.4-Hz waves and 3.5 m/s is sufficient to excite 0.6-Hz waves.

The winds exceed 3.5 m/s across great regions of the Pacific most of the time, therefore the microseism spectrum at frequencies above about 0.6 Hz will virtually always be near equilibrium. The spectra are "saturated" and all measurements look the same except during wide-spread calms. The *e*-folding distance above 0.6 Hz is of order 100 km, so an area of calms must be of the order of several hundred kilometers in radius for the microseism spectrum at the center of the region to fall much below the equilibrium microseism spectrum. We look to climatological atlases to assess how common regions of widespread calms are in World's oceans (U.S. Navy, 1977). At ocean station "Papa" in the Gulf of Alaska, we find that in January the winds exceed 3.5 m/s (7 kn) 95% of the time and even in July, the winds exceed 3.5 m/s 85% of the time. Near Hawaii, the fraction of time above 3.5 m/s is 88% in January and 95% in July, when trades are strongest. One of the quietest parts of the North Pacific in January seems to be along the East Pacific Rise, where the wind exceeds 3.5 m/s, a mere 79% of the time in January (68% in July).

In contrast, large regions of calms seem to be common in the central north Atlantic during the summer months. A station near the intersection of the Mid-Atlantic ridge and the Oceanographer transform fault sees winds of less than 3.5 m/s 47% of the time in July. At this station, we can expect to see intervals of very low noise during the Summer at frequencies from 0.6 Hz up to about 5 Hz since shipping becomes an important source of noise above about 5 Hz. Intervals of very low noise in this band have been seen in Eastern Pacific microseism data during calms, but these periods are usually short. There is little published microseism data from stations in the Atlantic. In the Winter, winds exceed 3.5 m/s across most of the North Atlantic virtually all of the time so we expect the microseism spectrum to be saturated at frequencies above 0.6 Hz throughout the Winter.

At lower frequencies, microseisms propagate farther, and the microseism spectrum depends more on where storms are over the oceans than on local conditions. The observations show most of the variability in the measured microseism spectrum occurs in a narrow band from 0.15 to 0.6 Hz corresponding to wind velocities for fully developed seas from 5 to 15 m/s, consistent with the usual range of winds over the ocean.

One of the most consistent differences between spectra from the Pacific and from the North Atlantic is an absence of microseisms at frequencies below about 0.14 Hz in the Atlantic, corresponding to ocean waves of 0.07 Hz and wind velocities of more than 20 m/s in the Neumann and Pierson model of a fully developed sea. At these low frequencies, the fetch required to reach the fully developed state is large, of order 600 km or more. Once generated, both ocean waves and microseisms at these very low frequencies will propagate enormous distances across the ocean with little attenuation.

Microseism energy declines precipitously at frequencies below 0.1 Hz. This lower limit is very stable, and results because ocean waves longer than 20-s period (0.05 Hz) almost never occur. Schillington (1981) describes a 0.045-Hz swell observed at Cape Town that may have generated 0.09-Hz microseisms. This location is exposed to large waves generated in the long fetches south and west of Africa, but even at this location, waves longer than 20-s period were only observed three times during an 8-yr span. The generation of 0.045-Hz waves requires sustained winds of over 30 m/s (60 kn) and a fetch of at least 1500 km. Fortunately, weather conditions such as this are rare even in the southern oceans.

There is a second mechanism that can generate microseisms at periods longer than 10 s, and causes a distinct second peak, the "single-frequency peak" seen on Atlantic seafloor records, and at land stations (Hasselmann, 1963). This mechanism is poorly understood and is ignored in this paper.

IX. COHERENCE BETWEEN INSTRUMENTS ON THE SEAFLOOR

The model presented here suggests that the microseism spectrum quickly evolves toward an equilibrium spectrum at frequencies above 0.3 Hz under source regions of only few

wnloaded 30 Jul 2011 to 134.246.166.168. Redistribution subject to ASA license or copyright; see http://asadl.org/journals/doc/ASALIB-home/info/terms.

hundred kilometers in extent. At equilibrium, the directional spectrum of each mode must be nearly isotropic, since the extent of the source region in every direction exceeds the typical e-folding distance associated with the relevant modes. The coherence between measurements from any pair of instruments on the seafloor falls off with horizontal separation quickly because of the absence of a preferred propagation direction in the microseism spectrum. The coherence between two vertical displacement sensors separated horizontally on the seafloor can be calculated using the equilibrium spectrum model. The coherence between vertical displacement measured at two points at depth h, separated by a horizontal distance r is

$$C_{ww}(\mathbf{r},\omega) = \langle w(\mathbf{x}+\mathbf{r},\omega) w(x,\omega)\rangle = \frac{\Sigma_n \int A_n(\theta,\omega) w_n^2(h) \exp[i\mathbf{k}\cdot\mathbf{r}] d\theta}{\Sigma_n \int A_n(\theta,\omega) w_n^2(h) d\theta}. \quad (38)$$

If the spectra are isotropic in direction then the integral over direction reduces to a Bessel function of order zero (Webb, 1986):

$$C_{ww} = \frac{\Sigma_n V_n(\omega) J_0(kr)}{\Sigma_n V_n(\omega)} \quad (39)$$

and the coherence is an energy weighted sum of Bessel functions with argument equal to the wave number of each mode times the separation distance. The V_n are the modal transfer functions [Eq. (32)].

The coherence calculated using an isotropic directional spectrum [Fig. 19(b)] is in general agreement with measurements from a site on the Pacific seafloor [Fig. 19(a)]. The amplitude of the coherence is shown as a function of both the distance between the two instruments and frequency. The most closely spaced instruments were 3 km apart. The coherence in the "single" frequency microseism peak between 0.05 and 0.1 Hz remains large to separations as great as 10 km. At intermediate frequencies in the double frequency microseism peak (0.15–0.5 Hz) the isotropic directional spectrum appears to correctly predict the fall off of coherence with distance as seen in the measurements. The models predicts less coherence than is seen in the measurements at the lowest frequencies (0.1 to 0.2 Hz) In this band, the microseism spectrum is controlled by Rayleigh waves from large storms, and the beam width of the directional spectrum is expected to be narrow (rather than isotropic).

Above 0.5 Hz, this model predicts greater coherence at separations less than 100 m than is seen in measurements (Schreiner and Dorman, 1990). Schreiner and Dorman (1990) have suggested significant energy is scattered at the rough rock–sediment interface into short wavelength waves propagating within the sediments (Stoneley modes) reducing the coherence. Because the energy in these modes is tightly confined to the seafloor, measurements of displacements made at the seafloor may be dominated by these modes, even if only a small fraction of the energy transport is associated with the Stoneley modes.

X. CONCLUSIONS

Microseisms are excited wherever the directional spectrum of ocean waves is sufficiently broad that pairs of surface gravity waves can couple energy into high phase velocity acoustic components in the ocean by nonlinear processes. Much of the surface of the World's ocean appears to be a source of microseisms at any time. This energy is trapped within a waveguide established by the seafloor and the steep gradients in elastic velocities in the crust and upper mantle. The source regions for microseisms are sufficiently large that a balance between excitation and dissipation within the waveguide must become established. Calculations of the excitation and dissipation of modes in this waveguide allows the equilibrium microseism spectrum to be calculated in any model ocean. These calculations closely follow measurements of microseism displacement and pressure spectra from the deep seafloor in both the Atlantic and the Pacific. Structure below the seafloor effects the equilibrium spectrum seen at a site. A thick layer of sediments reduces the amplitude of the seafloor pressure spectrum by about 10 dB, a consequence of greater attenuation within the sediments.

Efficient propagation within the ocean waveguide main-

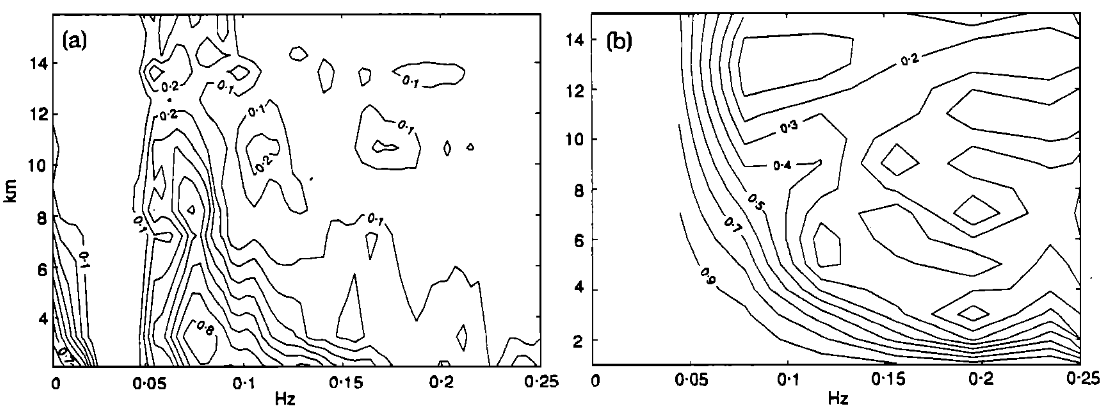

FIG. 19. (a) Contours of coherence amplitude as a function of frequency and distance between sensors measured with an array of pressure transducers on the seafloor in the eastern Pacific Ocean. (b) The coherence between sensors as a function of distance between sensors and frequency derived from the equilibrium spectrum model.

wnloaded 30 Jul 2011 to 134.246.166.168. Redistribution subject to ASA license or copyright; see http://asadl.org/journals/doc/ASALIB-home/info/terms

tains microseism amplitudes near the equilibrium spectrum even in large regions of calm winds, particularly at frequencies below about 0.6 Hz. The distances associated with one e-folding due to attenuation range from tens to thousands of kilometers from high to low frequency. Regions as small as 100 km are sufficient to excite microseism amplitudes within a few dB of the equilibrium values above 0.6 Hz. In contrast at lower frequencies, the spectrum will usually be 5 to 10 dB below the equilibrium values because of the finite size of the source region.

The microseism wave field has many similarities to the ocean surface wave field. Storms in localized regions establish an approximately saturated spectrum of ocean waves. As one moves out of the source region, the spectrum decays, with the highest frequencies lost first, while the lowest frequency waves persist to crash on shorelines all the way around the Pacific. Like microseisms, the long-range propagation of certain components means the sea surface is virtually never perfectly quiet anywhere in the Pacific. Again, like microseisms, the ocean wave spectrum measured at a site may be partly local, and partly "teleseismic." If one measures the pressure spectrum under ocean waves, one will see both a wave component and a component that is associated with pressure fluctuations in the atmosphere overhead. This component is equivalent to the "nonresonant" component referred to in the discussion of microseisms, however the "Q's" of ocean waves are so large, that the nonresonant component is nearly always infinitesimal compared to the "modal" component.

ACKNOWLEDGMENTS

This work was supported by the Office of Naval Research (N00014-90-J-1088). I thank Chip Cox and an anonymous reviewer for their reviews of the paper.

Adair, R. G., Orcutt, J. A., and Jordan, T. H. (1984). "Analysis of ambient seismic noise recorded by downhole and ocean-bottom seismometers on deep sea drilling project leg 78B," Init. Rep. Deep Sea Drill. Proj. 78, 767–780.

Adair, R. G. (1985). "Microseisms in the deep ocean: observations and theory," Ph.D. thesis, University of California, San Diego, 166 pp.

Aki, K., and Richards, P. G. (1980). *Quantitative Seismomology: Theory and Methods* (Freeman, San Francisco), p. 298.

Cox, C. S., and Jacobs, D. C. (1989). "Cartesian diver observations of double frequency pressure fluctuations in the upper levels of the ocean," Geophys. Res. Lett. 16(8), 807–810.

Donelan, M. A., Hamilton, J., and Hui, W. H. (1985). "Directional spectra of wind generated waves," Philos. Trans. R. Soc. London, Ser. A 315, 509–562.

Dougherty, M. E., and Stephens, R. A. (1988). "Seismic energy partitioning and scattering in laterally heterogeneous ocean crust," Pure Appl. Geophys. 128, 195–229.

Duennenbier, F. K., Cessaro, R. K., and Anderson, P. (1986). "Geoacoustic noise levels in a deep ocean borehole," in *Ocean Seismo-Acoustics* (Plenum, New York), pp. 743–751.

Gomberg, J. S., and Masters, T. G. (1987). "Waveform modeling using locked-mode synthethic and differential seismograms: application to determination of the structure of Mexico," Geophys. J. 94, 193–218.

Hasselmann, K. A. (1963). "A statistical analysis of the generation of microseisms," Rev. Geophys. Space Phys. 1, 177–210.

Hasselmann K. A., Barnett, T. P., Bouws, E., Carlson, H., Cartwright, P. E., Enke, K., Ewing, J. A., Gienapp, H., Hasselmann, D. E., Kruseman, P., Meerburg, A., Muller, P., Olbers, D. J., Richter, K., Sell, W., and Walden, H. (1973). "Measurements of wind-driven growth and swell decay during the joint North Sea wave project (JONSWAP)," Dtsch. Hydrogr. Inst., Hamburg 12, 95 pp.

Jacobs, D. C., Cox, C. S., and Zhang, X. (1990). "Observations of the near-field double frequency pressure spectrum in the upper ocean using the Cartesian Diver profiling instrument," in *Proceedings of Natural Physical Sources of Sound*, Cambridge, edited by B. Kerman (Kluwer, Dordrecht, The Netherlands).

Kennett, B. L. N. (1990). "Guided wave attenuation in laterally varying media," Geophys. J. Int. 100, 415–422.

Kibblewhite, A. C., and Ewans, K. C. (1985). "Wave-wave interactions, microseisms and infrasonic ambient noise in the ocean," J. Acoust. Soc. Am. 78, 981–994.

Kibblewhite, A. C., and Wu, C. Y. (1991), "The theoretical description of wave-wave interactions as a noise source in the ocean," J. Acoust. Soc. Am. 89, 2241–2252.

Kim, I. I., Smith, D. K., Orcutt, J. A., Jordan, T. H., and Menard, H. W. (1987). "Seismic relection site survey: correlation with physical properties, Leg 91, Deep Sea Drilling Project," Init. Rep. Deep Sea Drill. Proj. 91, 271–305.

Kohler, W., and Papanicolaou, G. C., (1977), "Wave propagation in a randomly inhomogeneous ocean," in *Wave Propagation and Underwater Acoustic*, edited by J. B. Keller and S. Papadakis (Springer-Verlag, Berlin), pp. 153–223.

Lighthill, J. (1978). *Waves in Fluids* (Cambridge U. P., Cambridge), p. 504.

Longuet-Higgins, M. S. (1950). "A theory for the generation of microseisms," Philos. Trans. R. Soc., Ser. A. 243, 1–35.

McCreery, C. S., and Duennebier, F. K. (1988). "The Holu spectrum: a worldwide deep-ocean constant, and indicator of the ocean wave spectrum," EOS 69, 1245.

McCreery, C. S., Duennebier, F. K., Walker, D. A., and Schroeder, T. A. (1991). "Long term ambient ocean noise, 0.05-30 Hz, from Wake Island hydrophones," EOS 72, 303.

Panza, G. F. (1985). "Synthetic seismograms: the Rayleigh wave modal summation," Geophysics 58, 125–145.

Pierson, W. J., and Moskowitz, L. (1964). "A proposed spectral form for fully developed wind seas based on the similarity theory of S. A. Kiaigorodskii," J. Geophys. Res. 69, 5181–5190.

Sauter, A. W. (1987). "Studies of the upper oceanic floor using ocean bottom seismometers," Ph.D. thesis, University of California, San Diego, 100 pp.

Schillington, F. A. (1981). "Low frequency 0.045 Hz swell from the southern ocean," Nature 290, 123–125.

Schmidt, H., and Kuperman, W. A. (1988). "Estimation of surface noise level from low frequency seismo-acoustic ambient noise measurements," J. Acoust. Soc. Am. 84, 2153–2162.

Schreiner, A. E., and Dorman, L. M. (1990). "Coherence lengths of seafloor noise: effect of bottom structure," J. Acoust. Soc. Am. 88, 1503–1514.

Shearer, P., and Orcutt, J. A. (1985). "Anistropy in the oceanic lithosphere-theory and observations from the Ngendei seismic refraction experiment in the southwest Pacific," Geophys. J. R. Astron. Soc. 80, 493–526.

Spudich, P., and Orcutt, J. A. (1980). "Petrology and porosity of an oceanic crustal site: results from wave modeling of seismic refraction data," J. Geophys. Res. 85, 1409–1433.

Tyler, G. L., Teague, C. C., Stewart, R. H., Peterson, A. M., Munk, W. H., and Joy, J. W. (1974). "Wave directional spectra from synthethic aperture observations of radio scatter," Deep Sea Res. 21, 989–1016.

U. S. Navy, *Marine Climatological Atlas of the World*, NAVAIR 50-1C-529 (U.S. Government Printing Office, Washington, DC, 1977).

Webb, S. C. and Cox, C. S. (1986), "Observations and modeling of seafloor microseisms," J. Geophys. Res. 91, 7343–7358.

Webb, S. C. (1986), "Coherent pressure fluctuations observed at two sites on the deep sea floor," Geophys. Res. Lett. 13, 141–144.

Webb, S. C. (1990). "Very low frequency sound studied using multi-element arrays," in *Proceedings of Natural Physical Sources of Sound*, Cambridge, edited by B. Kerman (Kluwer, Dordrecht, The Netherlands).

Webb, S. C. (1991). "Measurements of the wavenumber-frequency spectrum of oceanic microseisms," Proc. IEEE Oceans Conf. 1, 102–107.

Webb, S. C., and Schultz, A. (1992). "Very low frequency ambient noise at the seafloor under the Beaufort Sea icecap," J. Acoust. Soc. Am. 91,

wnloaded 30 Jul 2011 to 134.246.166.168. Redistribution subject to ASA license or copyright; see http://asadl.org/journals/doc/ASALIB-home/info/terms.

1429–1439.
Wilcock, W. S. D., Dougherty, M. E., Solomon, S. C., Toomey, D. R., and Purdy, G. R. (**1991**). "Finite difference models of wave propagation at 9°30′N: an evaluation of tomographic images of attenuation," EOS **72**, 495.
Woodhouse, J. H. (**1980**). "Efficient and stable methods for performing seismic calculations in stratified media," in *Proceedings of the International School of Physics Enrico Fermi Course* (North Holland, Amsterdam), Vol. 78, pp. 127–151.

wnloaded 30 Jul 2011 to 134.246.166.168. Redistribution subject to ASA license or copyright; see http://asadl.org/journals/doc/ASALIB-home/info/terms